Analysis of Dirac and Weyl points in topological semimetals via oscillation effects

G. P. Mikitik and Yu. V. Sharlai

B. Verkin Institute for Low Temperature Physics and Engineering of the National Academy of Sciences of Ukraine
Kharkiv 61103, Ukraine
E-mail: mikitik@ilt.kharkov.ua

We calculate the extremal cross-sectional areas and cyclotron masses for the Fermi-surface pockets in Dirac and Weyl topological semimetals. The calculation is carried out for the most general form of the electron energy bands in the vicinity of the Weyl and Dirac points. Using the obtained formulas, one can find parameters characterizing the Dirac and Weyl electrons in the topological semimetals from appropriate experimental data. As an example, we consider the W1 electrons in TaAs.

Keywords: topological semimetals, Weyl point, Dirac point, TaAs, oscillation effects in Weyl semimetals.

The topological Weyl and Dirac semimetals have attracted much attention in recent years; see, e.g., reviews [1–5] and references therein. In the Weyl semimetals, two electron bands contact at discrete (Weyl) points of the Brillouin zone and disperse linearly in all directions around these specific points. The same type of the band contact occurs in the Dirac semimetals, but the bands are double degenerate in spin. In other words, a Dirac point can be considered as a superposition of two Weyl points in the quasi-momentum space. The chemical potential of electrons ζ in the Weyl and Dirac semimetals is close to the band-contact energy ε_d. A number of the Dirac and Weyl semimetals were discovered in recent years [1, 2, 6].

Various oscillation effects are widely used in experimental investigations of the topological semimetals. In particular, measurements of the quantum-oscillations phase related to the so-called Berry phase [7] were carried out in a host of works in order to detect the Weyl and Dirac electrons in semimetals, see, e.g., review [5] and references therein. Beside this, using the Shubnikov–de Haas and de Haas–van Alphen effects, the extremal cross-sectional areas of the Fermi surfaces and the cyclotron masses corresponding to these cross-sections were measured for a number of the Weyl [8–15] and Dirac [16–25] semimetals. In this paper we present formulas for such areas and masses. These formulas will allow one to obtain the parameters characterizing the Dirac and Weyl points in the topological semimetals from the experimental data.

The most general electron dispersion relations $\varepsilon_{c,v}(\mathbf{p})$ of the two bands c, v in the vicinity of a Weyl (Dirac) point look as follows [5, 26, 27]:

$$\varepsilon_{c,v}(\mathbf{p}) = \varepsilon_d + \mathbf{a} \cdot \mathbf{p} \pm E(\mathbf{p}), \qquad (1)$$

where the quasi-momentum $\mathbf{p}$ is measured from this point, and $[E(\mathbf{p})]^2$ is a positively definite quadratic form in the components of the vector $\mathbf{p}$. Below we shall choose the coordinate axes along principal directions of this form. In this case, one has

$$[E(\mathbf{p})]^2 = b_{11} p_1^2 + b_{22} p_2^2 + b_{33} p_3^2, \qquad (2)$$

where b_{11}, b_{22}, b_{33} are the positive constants. The scaling of the coordinate axes, $\tilde{p}_i = p_i \sqrt{b_{ii}}$, transforms Eqs. (1), (2) into the form,

$$\varepsilon_{c,v} = \varepsilon_d + \tilde{\mathbf{a}} \cdot \tilde{\mathbf{p}} \pm |\tilde{\mathbf{p}}|,$$

that depends only on the constant dimensionless vector

$$\tilde{\mathbf{a}} \equiv \left(\frac{a_1}{\sqrt{b_{11}}}, \frac{a_2}{\sqrt{b_{22}}}, \frac{a_3}{\sqrt{b_{33}}} \right).$$

The vector $\tilde{\mathbf{a}}$ characterizes a tilt of the bands $\varepsilon_{c,v}(\mathbf{p})$, and its length is the most important parameter of dispersion relation (1). When the length of $\tilde{\mathbf{a}}$ is less than unity,

$$\tilde{a}^2 = \frac{a_1^2}{b_{11}} + \frac{a_2^2}{b_{22}} + \frac{a_3^2}{b_{33}} < 1,$$

the dispersion relations $\varepsilon_{c,v}(\mathbf{p})$ looks like in Fig. 1(a). In this case, the Fermi surface is either a closed hole pocket if $\zeta < \varepsilon_d$ or a closed electron pocket if $\zeta > \varepsilon_d$. When $\tilde{a}^2 > 1$, there is a direction in the $\mathbf{p}$-space along which the dispersion
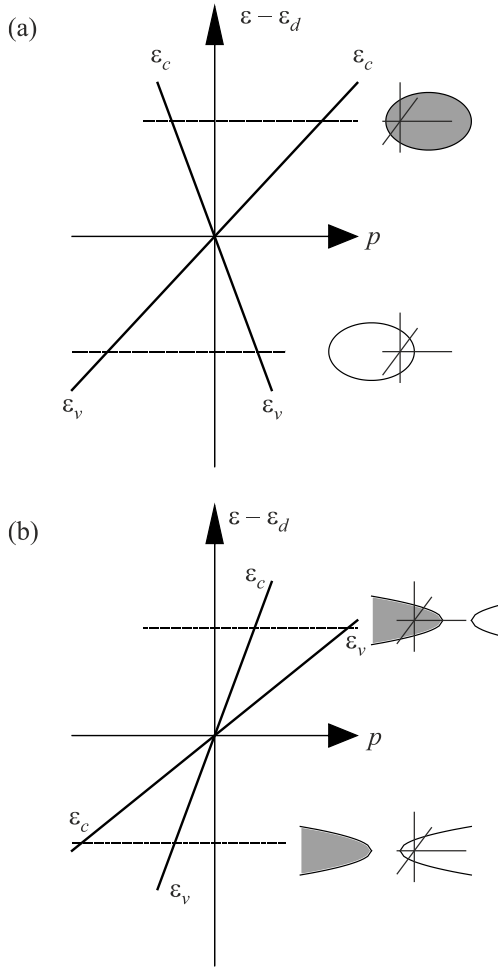
(a)

(b)

Fig. 1. Dispersion relations $\varepsilon_c(p)$ and $\varepsilon_v(p)$ of the two contacting bands in the vicinity of a Weyl (Dirac) point in the cases of $\tilde{a}^2 < 1$ (a) and $\tilde{a}^2 > 1$ (b). On the right, the Fermi surfaces at $\zeta - \varepsilon_d < 0$ and $\zeta - \varepsilon_d > 0$ are shown together with the Weyl (Dirac) point which is the origin of the coordinate axes. The shaded and white surfaces correspond to the electron and hole charge carriers, respectively.

relations $\varepsilon_{c,v}(\mathbf{p})$ look like in Fig. 1(b), and "open" electron and hole pockets of the Fermi surface exist both at $\zeta < \varepsilon_d$ and $\zeta > \varepsilon_d$. It is necessary to emphasize that the parameter $\tilde{a}^2$, which specifies the tilt of the bands, differs from zero for all the Weyl points and for the Dirac points induced by the band inversion [1] since all these points do not belong to the class of highly-symmetric points in the Brillouin zone of the topological semimetals. If $\tilde{a}^2 < 1$, a Weyl (Dirac) semimetal falls into the type I, whereas the case $\tilde{a}^2 > 1$ corresponds to the so-called type II Weyl (Dirac) semimetals [28]. Below we consider only the type I semimetals which have the closed Fermi surfaces.

At small $|\zeta - \varepsilon_d|$, the Fermi surfaces near the Weyl (Dirac) points are ellipsoids, with the center of the ellipsoids being displaced from these points (i.e., from $\mathbf{p} = 0$) by the vector that is proportional to $(\zeta - \varepsilon_d)$. Beside this, if at least two components of $\tilde{\mathbf{a}}$ differ from zero, the axes of the ellipsoid deviate from the axes of the coordinate system.

The displacement of the Fermi surface leads to the fact that its maximal cross-section perpendicular to a unit vector $\mathbf{n}$ generally does not pass through the Weyl (Dirac) point $\mathbf{p} = 0$, Fig. 1. Using the dispersion relation (1), (2), one can calculate both the maximal cross-sectional area $S_{\max}$ of the Fermi surface at an arbitrary direction $\mathbf{n}$ of the magnetic field H and the cyclotron mass $m_* = (1/2\pi)(\partial S_{\max}/\partial \zeta)$ corresponding to this cross-section,

$$S_{\max} = \frac{\pi(\zeta - \varepsilon_d)^2}{R_n^{1/2}(1 - \tilde{a}^2)}, \qquad (3)$$

$$m_* = \frac{(\zeta - \varepsilon_d)}{R_n^{1/2}(1 - \tilde{a}^2)}. \qquad (4)$$

The angular-dependent factor R_n in these expressions has the form,

$$R_n = b_{11}b_{22}b_{33}[(1 - \tilde{a}^2)\tilde{\mathbf{n}}^2 + (\tilde{\mathbf{a}} \cdot \tilde{\mathbf{n}})^2] = \sum_{i,j=1}^{3} \kappa^{ij} n_i n_j, \qquad (5)$$

where

$$\tilde{\mathbf{n}} \equiv \left(\frac{n_1}{\sqrt{b_{11}}}, \frac{n_2}{\sqrt{b_{22}}}, \frac{n_3}{\sqrt{b_{33}}} \right),$$

$$\kappa^{ij} = \frac{b_{11}b_{22}b_{33}}{(b_{ii}b_{jj})^{1/2}} \left[(1 - \tilde{a}^2)\delta_{ij} + \tilde{a}_i \tilde{a}_j \right],$$

and δ_{ik} is the Kronecker symbol. It follows from Eqs. (3) and (4) that

$$|\zeta - \varepsilon_d| = \frac{S_{\max}}{\pi |m_*|} = \frac{2e\hbar F}{c|m_*|}, \qquad (6)$$

where F is the frequency of the quantum oscillations produced by the cross-sectional area $S_{\max}$ in a physical quantity Q [i.e., the first harmonic of Q is proportional to $\cos(2\pi F/H + \phi_0)$, where ϕ_0 is some phase]. Therefore, if the frequency F and the cyclotron mass m_* have been measured at least for one direction of the magnetic field, formula (6) enables one to find the position of the chemical potential ζ relative to the energy ε_d of the Weyl (Dirac) point.

The dispersion relations (1), (2) is determined by the six parameters: b_{11}, b_{22}, b_{33}, $\tilde{a}_1$, $\tilde{a}_2$, $\tilde{a}_3$. Beside this, the orientation of the principal axes of the quadratic form $[E(\mathbf{p})]^2$ relative to the crystallographic axes of the semimetal can be described by three angles, and hence the nine parameters define a Weyl (Dirac) point in the general case. The angular dependenses of the frequency F are specified by the factor $1/\sqrt{R_n}$ in Eq. (3), and this factor is defined by the six constants κ^{ij}. Hence, an approximation of experimental angular dependences of this frequency with formulas (3), (5) together with Eq. (6) provides possibility to determine the six combinations of the parameters characterizing the dispersion relation.

The densities n_W and n_D of the Weyl and Dirac charge carriers can be expressed in terms of directly-measurable frequencies of the quantum oscillations,

$$n_W = \frac{N_W V}{(2\pi\hbar)^3}, \qquad n_D = \frac{2 N_D V}{(2\pi\hbar)^3}, \qquad (7)$$

where V is the volume of a Weyl or Dirac pocket in the Brillouin zone,

$$V = \frac{4[S_{max}^{(1)} S_{max}^{(2)} S_{max}^{(3)}]^{1/2}}{3\pi^{1/2}} = \frac{8\sqrt{2}\pi(e\hbar)^{3/2}(F_1 F_2 F_3)^{1/2}}{3c^{3/2}}, \quad (8)$$

N_W and N_D are the numbers of the equivalent pockets, F_1 and F_3 are the maximal and minimal frequencies produced by the pocket when the magnetic field rotates in various planes, and F_2 corresponds to the direction of $\mathbf{H}$ perpendicular to the directions at which F_1 and F_2 occur. The cross-sectional areas $S_{max}^{(i)}$ correspond to the frequencies F_i, and these cross-sections are mutually orthogonal.

Consider now two special cases in more detail.

1. Dirac point

In the Dirac semimetals induced by the band inversion, the Dirac points can lie only in symmetry axes of the third, fourth or sixth order [1]. The well-known Dirac semimetals Na$_3$Bi and Cd$_3$As$_2$ just fall into this class. In this case, one of the principal axes of $[E(\mathbf{p})]^2$ coincides with the symmetry axis, which we designate as the axis 3. The symmetry also imposes the restrictions: $b_{11} = b_{22} = b_\perp$ (generally $b_\perp \ne b_{33}$), $\mathbf{a} = (0,0,a_3)$. With these restrictions, formulas (3) and (5) give the following expressions for $S_{max}(\theta)$, the maximal area of the cross-section that is perpendicular to the magnetic field tilted at the angle θ to the symmetry axis,

$$S_{max}(0) = \frac{\pi(\zeta - \varepsilon_d)^2}{b_\perp(1 - \tilde{a}_3^2)}, \qquad (9)$$

$$\frac{S_{max}(\theta)}{S_{max}(0)} = \frac{1}{\sqrt{\cos^2\theta + \varepsilon^2 \sin^2\theta}}, \qquad (10)$$

where $\varepsilon^2 = (1 - \tilde{a}_3^2)b_{33}/b_\perp$. Thus, if $S_{max}(0)$, $m_*(0)$, $S_{max}(\pi/2)$ are measured, one can find $|\zeta - \varepsilon_d|$, $b_\perp(1 - \tilde{a}_3^2)$, and ε with formulas (6), (9), (10). Note that dependence (10) has the standard form typical of an ellipsoidal Fermi surface. However, the anisotropy of the Fermi surface $\varepsilon = S_{max}(0)/S_{max}(\pi/2)$ contains the factor $\sqrt{1 - \tilde{a}_3^2}$ which is caused by the tilt of the bands $\varepsilon_{c,v}(\mathbf{p})$. The density n_D of the Dirac charge carriers can be found with Eqs. (7), (8) where $S_{max}^{(1)} S_{max}^{(2)} S_{max}^{(3)} = S_{max}(0)[S_{max}(\pi/2)]^2$ now.

2. Weyl point near a reflection plane

Consider a Weyl point for which the parameters meet the following restrictions: $b_{11}, b_{22} \gg b_{33}$ and $a_3 \ll a_1$, but

$\tilde{a}_3 \equiv a_3/\sqrt{b_{33}}$ can have any value satisfying the condition $(\tilde{a}_3)^2 < 1 - (\tilde{a}_1)^2 - (\tilde{a}_2)^2$. Such a point may appear if it results from a nodal line that lies in the reflection plane 1-3 of the crystal without the inversion symmetry. This line exists in neglect of the spin-orbit interaction. In this case, for any point of the line, the vector $\mathbf{a}$ lies in the reflection plane (i.e., $a_2 = 0$), whereas one of the local values of b_{11}, b_{33} is equal to zero (for definiteness, let $b_{33} = 0$) [5, 26, 27]. A nonzero strength of spin-orbit interaction lifts the degeneracy of the electron bands along the nodal line and can lead to the appearance of two Weyl points disposed near the reflection plane (symmetrically relative to it) [11]. If the spin-orbit interaction does give rise to the Weyl point slightly displaced from the plane, one may expect that a_1, a_3, b_{11}, b_{33} will experience small changes, and the condition b_{11}, $b_{22} \gg b_{33}$ will hold true for the point. The fact of the appearance of the closed Fermi pocket surrounding the Weyl point provides the fulfilment of the condition $(\tilde{a}_3)^2 < 1 - (\tilde{a}_1)^2 - (\tilde{a}_2)^2$ which means that such a pocket can occur near the point of the line where a_3 is relatively small, $a_3 \lesssim \sqrt{b_{33}} \ll \sqrt{b_{11}} \sim a_1$. Although one may also expect that $\tilde{a}_2 \approx 0$ for the Weyl point, the closeness of the two Weyl points to each other may noticeably modify the values of b_{22} and $\tilde{a}_2$, and so we do not impose any restriction on these parameters.

For the Weyl point that results from the nodal line, the perpendicular to this line in the reflection plane, the normal to the plane, and the direction along the line are close to the directions of the axes 1, 2, and 3, respectively. In Fig. 2 we show the angular dependences of the frequency $F(\theta) = c S_{max}(\theta)/(2\pi\hbar e)$, where θ is the angle between the magnetic field and the axis 3. This angle changes either in the 1-3 plane or in the 2-3 plane. Since in a tetragonal crystal like TaAs, the equivalent Weyl pockets exist near the two perpendicular reflection planes, both the dependences
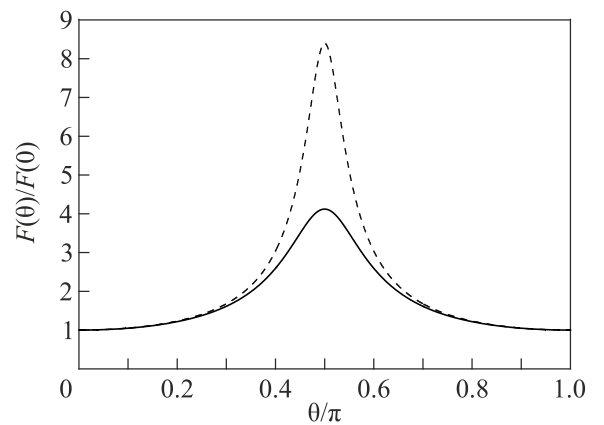

Fig. 2. The frequency of quantum oscillations, $F = c S_{max}/(2\pi e\hbar)$, versus the angle θ between the direction of the magnetic field and the axis 3, Eqs. (3) and (5). Here $\tilde{a}_1 = 0.5$, $\tilde{a}_2 = 0.47$, $\tilde{a}_3 = 0$, $b_{22}/b_{11} = 4$, $b_{33}/b_{11} = 0.04$ (these values correspond to the first set of the parameters in Table 1). The angle θ changes either in the 1-3 plane (the solid line) or in the 2-3 plane (the dashed line).

presented in Fig. 2 can be observed for H rotating in each of the planes. In particular, the dependences shown in Fig. 2 are similar to those found for the so-called W1 electrons in TaAs (see Fig. 3(a) in Ref. 11). In Fig. 2 we take $\tilde{a}_3 = 0$. If $\tilde{a}_3 \neq 0$, the minimum value of $F(\theta)$ is reached at the non-zero angle θ_m in the plane 1-3,

$$\theta_m \approx \frac{\tilde{a}_1 \tilde{a}_3}{1 - \tilde{a}_1^2 - \tilde{a}_2^2} \sqrt{\frac{b_{33}}{b_{11}}}. \qquad (11)$$

A similar formula describes the position of the minimum of $F(\theta)$ in the plane 2-3 (in this case, $\tilde{a}_1$, $\tilde{a}_2$, and b_{11} are replaced by $\tilde{a}_2$, $\tilde{a}_1$, and b_{22}, respectively). These nonzero θ_m are due to the above-mentioned deviation of the Fermi-surface axes from the coordinate axes.

3. Example: W1 electrons in TaAs

As an example, let us analyze the known experimental data for the W1 electrons in the Weyl semimetal TaAs [11]. Near the W1 points the appropriate nodal lines are parallel to the c axis, and therefore it is reasonable to suppose that the directions of the axes 1, 2, 3 coincide with the directions of the crystallographic axes a, b, c. Arnold *et al.* [11] found that the frequency of quantum oscillations F changes like in Fig. 2 when the direction of the magnetic field varies in the reflection plane c-a from the c axis ($\theta = 0$) to the a axis ($\theta = \pi/2$), and they obtained $F(0) \approx 7$ T, $m_*(0)/m \approx 0.057$. At $\theta \neq 0$, the frequency $F(\theta)$ splits into the two branches $F_a(\theta)$, $F_b(\theta)$ associated with the ellipsoids lying near the axes a and b (Fig. 3), and the frequencies $F_a(\pi/2)$ and $F_b(\pi/2)$ take the values 29 and 59 T. Using formula (6) and the values of $F(0)$ and $m_*(0)$, we arrive at $\zeta - \varepsilon_d \approx 28.4$ meV. This result is close to the value 26 meV obtained in the band-structure calculations [11]. Using Eq. (6), we can also predict the values of the cyclotron masses $m_*(\pi/2)/m \approx 0.24$ and 0.48 which correspond to the frequencies 29 and 59 T, respectively.

With $\zeta - \varepsilon_d \approx 28.4$ meV and Eqs. (3), we find $R_n^{1/2}(1 - \tilde{a}^2)$ at $\theta = 0$,

$$R_c^{1/2}(1 - \tilde{a}^2) = \frac{c(\zeta - \varepsilon_d)^2}{2e\hbar F(0)} \approx 8.75 \cdot 10^{10} \frac{m^2}{s^2},$$

where $R_c \equiv R_n |_{\theta=0}$. On the other hand, Eq. (5) gives

$$R_c^{1/2}(1 - \tilde{a}^2) \approx \sqrt{b_{11} b_{22}(1 - \tilde{a}_1^2 - \tilde{a}_2^2)}(1 - \tilde{a}^2), \qquad (12)$$

and hence we have found the value of the right hand side of this expression.

According to Eq. (5), the factor $R_n^{1/2}$ at $\theta = \pi/2$ looks like

$$\sqrt{R_a} \approx \sqrt{b_{22} b_{33}(1 - \tilde{a}_2^2 - \tilde{a}_3^2)},$$

$$\sqrt{R_b} \approx \sqrt{b_{11} b_{33}(1 - \tilde{a}_1^2 - \tilde{a}_3^2)},$$

for the W1 ellipsoids lying near the a and b axes, respectively. Since there are no visible displacements of the minima of $F_a(\theta)$ and $F_b(\theta)$ from the point $\theta = 0$ in Fig 3(a) of Ref. 11, we conclude that the parameter $\tilde{a}_3$ is small for the W1 electrons, i.e., $\tilde{a}_3 \approx 0$, and so $\tilde{a}^2 \approx (\tilde{a}_1)^2 + (\tilde{a}_2)^2$. Therefore, the ratios $R_c^{1/2}/R_a^{1/2}$ and $R_c^{1/2}/R_b^{1/2}$ reduce to

$$\sqrt{\frac{b_{11}(1 - \tilde{a}_1^2 - \tilde{a}_2^2)}{b_{33}(1 - \tilde{a}_2^2)}}, \quad \sqrt{\frac{b_{22}(1 - \tilde{a}_1^2 - \tilde{a}_2^2)}{b_{33}(1 - \tilde{a}_1^2)}}. \qquad (13)$$

However, these ratios determine $F_a(\pi/2)/F(0)$, $F_b(\pi/2)/F(0)$, and so they are equal to 29/7 and 59/7 (or 59/7 and 29/7). Thus, we have found the values of the two combinations of the parameters (13).

When the magnetic field rotates in the a-b plane from the a axis ($\phi = 0$) to the direction $[110]$ ($\phi = \pi/4$), each of the frequencies $F_a(\phi)$ and $F_b(\phi)$ splits into the two branches $F_{a1}(\phi)$, $F_{a2}(\phi)$ and $F_{b1}(\phi)$, $F_{b2}(\varphi)$ if $\tilde{a}_2 \neq 0$, i.e., if the principal axes of the ellipsoids deviate from the a and b axes. The ϕ-dependences of these four branches are determined by the factors,

$$R_{a1,a2}(\phi) = b_{11} b_{33}(1 - \tilde{a}_1^2)\sin^2\phi + b_{22}b_{33}(1 - \tilde{a}_2^2)\cos^2\phi \pm$$
$$\pm 2\sqrt{b_{11}b_{22}} b_{33} \tilde{a}_1 \tilde{a}_2 \sin\phi\cos\phi, \qquad (14)$$

$$R_{b1,b2}(\phi) = b_{11} b_{33}(1 - \tilde{a}_1^2)\cos^2\phi + b_{22}b_{33}(1 - \tilde{a}_2^2)\sin^2\phi \pm$$
$$\pm 2\sqrt{b_{11}b_{22}} b_{33} \tilde{a}_1 \tilde{a}_2 \sin\phi\cos\phi. \qquad (15)$$

At $\phi = 0$, the two factors $R_{a1}(\phi)$ and $R_{a2}(\phi)$ reduce to R_a, whereas $R_{b1}(0)$ and $R_{b2}(0)$ coincide with R_b. When $\phi = \pi/4$, the four frequencies partly merge again since $R_{a1}(\pi/4) = R_{b1}(\pi/4)$ and $R_{a2}(\pi/4) = R_{b2}(\pi/4)$. It is evident from Eqs. (14) and (15) that at any ϕ,

$$R_{a1}(\phi) + R_{a2}(\phi) + R_{b1}(\phi) + R_{b2}(\phi) = 2R_a + 2R_b.$$

This equality leads to the relation between the appropriate four branches of the frequency,

$$\frac{1}{[F_{a1}(\phi)]^2} + \frac{1}{[F_{a2}(\phi)]^2} + \frac{1}{[F_{b1}(\phi)]^2} + \frac{1}{[F_{b2}(\phi)]^2} = \frac{2}{[F_a]^2} + \frac{2}{[F_b]^2}, \qquad (16)$$
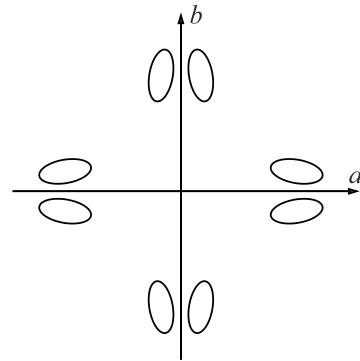
Fig. 3. The outline of the cross-sections of the W1 ellipsoids by the a-b plane in TaAs.

where F_a and F_b are equal to 29 and 59 T. According to Fig. 3(a) in Ref. 11, $F_{a1}(\pi/4) = F_{b1}(\pi/4) \approx 33$ T. This condition gives the fourth relation on the five parameters $\tilde{a}_1$, $\tilde{a}_2$, b_{11}, b_{22}, and b_{33},

$$\frac{[R_c]^{1/2}}{[R_{a1}(\pi/4)]^{1/2}} = \frac{F_{a1}(\pi/4)}{F(0)} \approx \frac{33}{7}. \quad (17)$$

Table 1. The two possible sets of the parameters specifying the W1 electrons in TaAs

Set	$\sqrt{b_{11}}$, 10^5 m/s	$\sqrt{b_{22}}$, 10^5 m/s	$\sqrt{b_{33}}$, 10^4 m/s	$\tilde{a}_1$	$\tilde{a}_2$	$\tilde{a}_3$
1	3.37	6.74	6.7	0.5	0.47	0
2	6.88	3.30	6.7	0.5	0.47	0

The parameter $\tilde{a}_1$ can be obtained from the band structure calculation along the a axis. In particular, Fig. 1 in Ref. 11 permits one to obtain the following crude estimate: $\tilde{a}_1 \approx 0.5$. Taking into account the above four relations between b_{11}, b_{22}, b_{33}, $\tilde{a}_1$, $\tilde{a}_2$, we find two possible sets of the parameters characterizing the W1 points in TaAs, Table 1. The dependences of the frequencies F_{a1}, F_{a2}, F_{b1}, F_{b2} on ϕ for the first set of the parameters are presented in Fig. 4.

At nonzero values of $\tilde{a}_1$ and $\tilde{a}_2$, the principal axes of the ellipsoid in the a-b plane deviate from the a and b axes (Fig. 3). A simple analysis leads to the following formula for the deviation angle ψ:

$$\tan(2|\psi|) = \frac{[F_{a2}(\pi/4)]^{-2} - [F_{a1}(\pi/4)]^{-2}}{[F_a]^{-2} - [F_b]^{-2}}, \quad (18)$$

where the value of $F_{a2}(\pi/4) = F_{b2}(\pi/4) \approx 42.3$ T can be found from Eq. (16). Using formula (18), we obtain
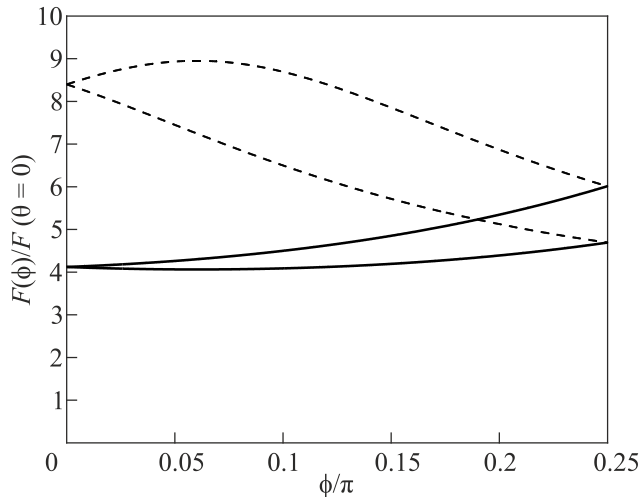

Fig. 4. The frequencies $F_{a1,a2}$ (the solid lines) and $F_{b1,b2}$ (the dashed lines) versus the angle ϕ between the a axis and the magnetic field lying in the a-b plane. The parameters are the same as in Fig. 2 (i.e., they coincide with the first set in Table 1).

$|\psi| \approx 11°$ or $|\psi| \approx 79°$. These two values of $|\psi|$ correspond to the two sets of the parameters in Table 1. For the first set, the orientation of the ellipsoids in the a-b plane is schematically shown in Fig. 3. In this case, the maximal axis of their cross-sections by the a-b plane is inclined at the angle of 11° to the a and b axes. For the second set, this angle is equal to 79°.

Knowing the angle ψ, the frequencies F_1 and F_2 in formula (8) can be calculated, and we arrive at

$$F_1 F_2 = F_a F_b \left[1 - \frac{(F_a^2 - F_b^2)^2}{4F_a^2 F_b^2}\tan^2(2|\psi|)\right]^{-1/2}. \quad (19)$$

Eventually, expressions (7), (8), (19) with $F_3 = F(\theta = 0) = 7$ T give the density $n_{W1} \approx 2.53 \cdot 10^{18}$ cm^{-3} produced by the eight equivalent pockets of the W1 electrons in TaAs.

————————

1. N. P. Armitage, E. J. Mele, and A. Vishwanath, *Rev. Mod. Phys.* **90**, 015001 (2018).

2. A. Bernevig, H. Weng, Z. Fang, and X. Dai, *J. Phys. Soc. Jpn.* **87**, 041001 (2018).

3. H. Gao, J. W. F. Venderbos, Y. Kim, and A. M. Rappe, *Annu. Rev. Mater. Res.* **49**, 153 (2019).

4. S. Wang, B.-C. Lin, A.-Q. Wang, D.-P. Yu, and Z.-M. Liao, *Adv. Phys.: X* **2**, 518 (2017).

5. G. P. Mikitik and Yu.V. Sharlai, *J. Low Temp. Phys.* **197**, 272 (2019).

6. C.-L. Zhang, C. M. Wang, Z. Yuan, X. Xu, G. Wang, C.-C. Lee, L. Pi, C. Xi, H. Lin, N. Harrison, H.-Z. Lu, J. Zhang, and S. Jia, *Nat. Commun.* **10**, 1028 (2019).

7. G. P. Mikitik and Yu.V. Sharlai, *Phys. Rev. Lett.* **82**, 2147 (1999).

8. X. Huang, L. Zhao, Y. Long, P. Wang, D. Chen, Z. Yang, H. Liang, M. Xue, H. Weng, Z. Fang, X. Dai, and G. Chen, *Phys. Rev. X* **5**, 031023 (2015).

9. Y. Luo, N. J. Ghimire, M. Wartenbe, H. Choi, M. Neupane, R. D. McDonald, E. D. Bauer, J. Zhu, J. D. Thompson, and F. Ronning, *Phys. Rev. B* **92**, 205134 (2015).

10. C. Shekhar, A. K. Nayak, Y. Sun, M. Schmidt, M. Nicklas, I. Leermakers, U. Zeitler, Yu. Skourski, J. Wosnitza, Z. Liu, Y. Chen, W. Schneller, H. Borrmann, Yu. Grin, C. Felser, and B. Yan, *Nat.Phys.* **11**, 645 (2015).

11. F. Arnold, M. Naumann, S.-C. Wu, Y. Sun, M. Schmidt, H. Borrmann, C. Felser, B. Yan, and E. Hassinger, *Phys. Rev. Lett.* **117**, 146401 (2016).

12. J. Hu, J. Y. Liu, D. Graf, S. M. A. Radmanesh, D. J. Adams, A. Chuang, Y. Wang, I. Chiorescu, J. Wei, L. Spinu, and Z. Q. Mao, *Sci. Rep.* **6**, 18674 (2016).

13. J. Du, H. Wang, Q. Chen, Q. Mao, R. Khan, B. Xu, Y. Zhou, Y. Zhang, J. Yang, B. Chen, C. Feng, and M. Fang, *Sci. China-Phys. Mech. Astron.* **59**, 657406 (2016).

14. Philip Sergelius, Johannes Gooth, Svenja Bäßler, Robert Zierold, Christoph Wiegand, Anna Niemann, Heiko Reith, Chandra Shekhar, Claudia Felser, Binghai Yan, and Kornelius Nielsch, *Sci. Rep.* **6**, 33859 (2016).

15. Z. Wang, Y. Zheng, Z. Shen, Y. Lu, H. Fang, F. Sheng, Y. Zhou, X. Yang, Y. Li, C. Feng, and Z.-A. Xu, *Phys. Rev. B* **93**, 121112 (2016).

16. L. P. He, X. C. Hong, J. K. Dong, J. Pan, Z. Zhang, J. Zhang, and S. Y. Li, *Phys. Rev. Lett.* **113**, 246402 (2014).

17. A. Pariari, P. Dutta, and P. Mandal, *Phys. Rev. B* **91**, 155139 (2015).

18. T. Liang, Q. Gibson, M. N. Ali, M. Liu, R. J. Cava, and N. P. Ong, *Nat. Mater.* **14**, 280 (2015).

19. Y. Zhao, H. Liu, C. Zhang, H. Wang, J. Wang, Z. Lin, Y. Xing, H. Lu, J. Liu, Y. Wang, S. M. Brombosz, Z. Xiao, S. Jia, X. C. Xie, and J. Wang, *Phys. Rev. X* **5**, 031037 (2015).

20. A. Narayanan, M. D. Watson, S. F. Blake, N. Bruyant, L. Drigo, Y. L. Chen, D. Prabhakaran, B. Yan, C. Felser, T. Kong, P. C. Canfield, and A. I. Coldea, *Phys. Rev. Lett.* **114**, 117201 (2015).

21. Z. J. Xiang, D. Zhao, Z. Jin, C. Shang, L. K. Ma, G. J. Ye, B. Lei, T. Wu, Z. C. Xia, and X. H. Chen, *Phys. Rev. Lett.* **115**, 226401 (2015).

22. W. Desrat, C. Consejo, F. Teppe, S. Contreras, M. Marcinkiewicz, W. Knap, A. Nateprov, and E. Arushanov, *J. Phys.: Conf. Ser.* **647**, 012064 (2015).

23. J. Cao, S. Liang, C. Zhang, Y. Liu, J. Huang, Z. Jin, Z.-G. Chen, Z. Wang, Q. Wang, J. Zhao, S. Li, X. Dai, J. Zou, Z. Xia, L. Li, and F. Xiu, *Nat. Commun.* **6**, 7779 (2015).

24. L.-P. He and S.-Y. Li, *Chin. Phys. B* **25**, 117105 (2016).

25. I. Crassee, R. Sankar, W.-L. Lee, A. Akrap, and M. Orlita, *Phys. Rev. Mater.* **2**, 120302 (2018).

26. G. P. Mikitik and I. V. Svechkarev, *Fiz. Nizk. Temp.* **15**, 295 (1989) [*Sov. J. Low Temp. Phys.* **15**, 165 (1989)].

27. G. P. Mikitik and Yu.V. Sharlai, *Fiz. Nizk. Temp.* **22**, 762 (1996) [*Low Temp. Phys.* **22**, 585 (1996)].

28. A. Soluyanov, D. Gresch, Z. Wang, Q. Wu, M. Troyer, X. Dai, and B. A. Bernevig, *Nature* **527**, 495 (2015).

_____

Аналіз точок Дірака та Вейля в топологічних напівметалах за допомогою осциляційних ефектів

G. P. Mikitik, Yu. V. Sharlai

Обчислено площі екстремальних перерізів та циклотронні маси поверхонь Фермі в діраківських та вейлівських топологічних напівметалах. Розрахунок проведено для найбільш загального випадку електронних енергетичних зон поблизу вейлівських та діраківських точок. Використовуючи отримані формули, можна знайти параметри, що характеризують діраківські та вейлівські електрони в топологічних напівметалах. Як приклад, розглянуто електрони W1 в TaAs.

Ключові слова: топологічні напівметали, точки Вейля, точки Дірака, TaAs, осциляційні ефекти у вейлівських напівметалах.